From droplets to particles: Transformation criteria

Victor Chéron, J C Brändle de Motta, G. Vaudor, T. Ménard, A. Berlemont

From droplets to particles: Transformation criteria

V. Chéron[1], J.C. Brändle de Motta[*,1], G. Vaudor[1], T. Ménard[1], A. Berlemont[1]
[1]CNRS UMR 6614-CORIA, Rouen Normandie Université,
Avenue de l'Université, Saint-Étienne-du-Rouvray, 76801, France
*Corresponding author: jorge.brandle@coria.fr

Abstract
Atomization of liquid fuel has a direct impact on the production of pollutant emission in engineering propulsion devices. Due to the multiple challenges in experimental investigations, motivation for numerical study is increasing on liquid-gas interaction from injection till dispersed spray zone. Our purpose is to increase the accuracy of the treatment of droplets in atomized jet, which are typically 100 times smaller than the characteristic injection length size. As the characteristic length reduces downstream to the jet, it is increasingly challenging to track the interface of the droplets accurately. To solve this multiscale issue, a coupled tracking Eulerian-Lagrangian Method exists [1]. It consists in transforming the small droplets to Lagrangian droplets that are transported with drag models. In addition to the size transformation criteria, one can consider geometric parameters to determine if a droplet has to be transformed. Indeed, the geometric criteria are there for two reasons. The first one is the case where the droplets can break if there are not spherical. The second one is about the drag models that are based on the assumption that the droplet is spherical. In this paper we make a review of the geometric criteria used in the literature. New geometric criteria are also proposed. Those criteria are validated and then discussed in academic cases and a 3D airblast atomizer simulation. Following the analysis of the results the authors advise the use of the deformation combined with surface criteria as the geometric transformation criteria.

Keywords
DNS, Multiscale, Droplets, Transformation Criteria, Deformation

Introduction

Atomization is a phenomenon encountered in many applications such as sprays in cosmetic engineering or aerospace engineering for jet propulsion [2]. In the combustion chamber, the total surface of the interface separating the two phases is a key parameter. Primary and secondary breakup have been extensively investigated in the literature. However, in order to fully describe the complete process, one has to capture droplets in dispersed zone 100 times smaller than jet diameter. Atomization is then a multiphase and a multiscale flow phenomenon which is still far from being understood.

Due to this wide range of scale, the Direct Numerical Simulation (DNS) of such process requires robust and efficient codes. DNS is an important tool to analyse the experimental results and go further into the atomization understanding. In the past few years, numerical schemes of Interface Capturing Method (ICM) have been improved but faced numerical limitation. For instance, the treatment of the small droplets is the most challenging part when the entire process is treated in DNS. When dealing with unresolved structures we face different problems such as the dilution or the creation of numerical instabilities. To avoir them, a strategy is to remove small structures during the simulation, see Shinjo et al. [3]. But, those methods do not collect information on smallest droplets in atomization application. Introduction of Adaptive Mesh Refinement (AMR) in DNS is a first answer to this issue, it consists in refining unresolved area under numerical concept and focus on the interface between two phases instead of refining the entire domain. In dense spray, AMR tends to refine the entire zone and becomes as expensive as a full domain refinement. A solution is to transform the smallest droplets into point particles and remove AMR in this area. This strategy is called Eulerian-Lagrangian coupling [1], it assumes that small droplets will no longer break during the simulation and that the Lagrangian models reproduce correctly the droplet transport. These physical assumptions are implemented to answer numerical issue and improve the computational cost. This Eulerian-Lagrangian coupling is based on transformation criteria that defines when an ICM structure has to be transformed into Lagrangian particle and when a Lagrangian particle has to be transformed back into ICM. The main purpose of the present communication is to provide a detailed analysis of the ICM to Lagrangian transformation criteria. The geometric criteria in [1] is based on the droplet's volume, *VOF*: $R_{eq} = R_{eq,VOF} = \left(\frac{3V_{VOF}}{4\pi}\right)^{1/3}$. If R_{EQ} is equal or smaller than the mesh size, Δx, transformation is applied. Based on the conclusion of Shinjo et al. [3] and previous work, Zuzio et al. [4], implemented a second Lagrangian tracking method to transform intermediate size droplets with $R_{EQ} \leqslant 4\Delta x$. Those coupling methods focus on unresolved droplets (i.e. small droplets compared to the mesh size) under the assumption that they are spherical. Because two different Lagrangian methods are used, new transformation criteria is used to quantify the sphericity. This criteria is adapted to intermediate size of unresolved structures and it can be enhanced by adding breakup criteria. For this kind of relations some models can be used, see Lasheras et al. [5]. To ensure that the Lagrangian transport is physical, it is also necessary to take into account the droplet stability.

In this communication, authors resume existing geometric criteria, compare them and propose new ones. After the introduction of our numerical approach, the methodology to determine geometrical information globally and

locally on our structures is described. Then, the accuracy of computation of the geometrical properties is analyzed on a spherical droplet. Next, their implementation on an oscillatory droplet case, following the Lamb theory, is studied to determine their capability to reproduce shape deformation. Then, we treat the case of a droplet in a pseudo-turbulent flow to produce surface variation and study the evolution of geometrical transformation criteria at low Weber number. Finally, a 3D airblast atomization has been performed to analyze the implemented criteria in a realistic case.

Numerical Methods

Our in-house multiphase code, *ARCHER*, is a DNS code which has strong experience in interface treatment and atomization process, Osmar 2014 et al. [10]. It solves incompressible Navier Stokes equation on a cubic staggered grid where the pressure and the velocity are decoupled. Interface is tracked with CLSVOF, *Coupled Level-set Volume of Fluid method*, Ménard et al. [6], coupling a *Level-set* distance function [7] and a *Volume of Fluid* (VOF) method. The *Level-set* function ϕ describes the interface at its zero level curve of a continuous function defined by the signed distance to the interface. To ensure that the function remains the signed distance to the interface, a redistancing algorithm is applied.

$$\frac{\partial d}{\partial t} = sign(\phi)(1 - |\nabla d|) \qquad \text{where} \qquad d(x,t,\tau)_{\tau=0} = \phi(x,t) \tag{1}$$

The redistanciation of the *Level-set* coupled with a sign function helps to determine the distance between various structures as it is shown on the top right part of the figure 1a. The CLSVOF method uses a ghost fluid method in order to capture sharp discontinuities at the interface, it is second order on the curvature. Distance information are illustrated on the top left part of the figure 1a. The *CLSVOF* is a second order method conservative in mass where the *VOF* represents the amount of each phase in a cell. A coupling ensures conservation of the mass, thanks to a robust advective scheme of the fluxes [8], its representation is illustrated on the down right part of the figure 1a, all cells have a percentage of volume represented in orange, their amount of *VOF*. The surface of a structure S_{VOF} is computed by adding the surface contained in each cell $S_{i,VOF}$. This local surface is approximated by the surface of the plane obtained from the volume of fluid and the normal. The normal to the surface, $\mathbf{n}$, and the curvature, κ, are related to *Level-set* function, see equation 2.

$$\mathbf{n} = \frac{\nabla\phi}{|\nabla\phi|}, \qquad \text{and} \qquad \kappa = -\nabla \cdot \mathbf{n}. \tag{2}$$

The two main curvatures, κ_1 and κ_2, at a given point of the surface are obtained from the work of Kindlmann et al. [9]. Here we average the main curvatures over the surface of the structure. This computation is done by using the curvature of each cell pondered by the interface surface, see equation 3.

$$\kappa_{1,S}(\phi) = \frac{\sum_i^{Ncell,tag} S_{i,VOF}\kappa_{1,i(\phi)}}{S_{VOF}} \qquad \text{and} \qquad \kappa_{2,S}(\phi) = \frac{\sum_i^{Ncell,tag} S_{i,VOF}\kappa_{2,i(\phi)}}{S_{VOF}}. \tag{3}$$

Tag represents the cells of a given structure from a tagging algorithm. Information that are obtained at the interface of the structure are resumed on the down right part of the figure 1a.

Viscous terms are discretized with Sussman algorithm. Projection method estimates spatial derivatives at a second order central scheme and convective terms are approximated by a fifth order WENO scheme. Pressure is obtained with a Poisson equation discretization and second order scheme is used. Sharp interface is described with a jump function for the pressure, density and viscosity in order to carefully describe all discontinuities. Eulerian-Lagrangian coupling is implemented in the in-house code with two Lagrangian tracking methods, as in Zuzio et al. [4].

Geometrical computation

To transform droplets into particles, geometrical properties are needed to characterize the structure. The *CLSVOF* method gives various information such as the total volume of a structure, the position of its interface, the distance to other interfaces, principal curvature or the total surface. Numerical algorithm have been implemented in the in-house code to recover geometric information, see figure 1a for a graphical overview. To determine all the cells belonging to the same structure $\mathbf{X}_{cell}$, the tag algorithm of Herrmann [1] is used. The center of mass of a structure $\mathbf{X}_{struct}$ is obtained from the amount of *VOF*, α_i, in a tagged cell centered in $\mathbf{x}_i$: $\mathbf{X}_{struct} = \sum_i^{Ncell,tagg} \alpha_i \mathbf{x}_i$. The strategy is to compute the equivalent radius that a structure would have if it was spherical. The *CLSVOF* method offer various possibilities and some are listed below. A first is to use the properties of the *VOF* to respect the mass conservation, and determine a $R_{EQ,VOF}$, similar to Herrmann [1]. The obtained equivalent spherical droplet is drawn in dashed green on the figure 1a. An equivalent radius can also be calculated with the total surface of the structure $R_{S_{VOF}} = \sqrt{\frac{S_{VOF}}{4\pi}}$. One can also use *Level-set* properties to determine an equivalent radius based on minimal curvatures, see equation 4.

$$R_\kappa = \frac{2}{\kappa_{1,S}(\phi) + \kappa_{2,S}(\phi)} \tag{4}$$

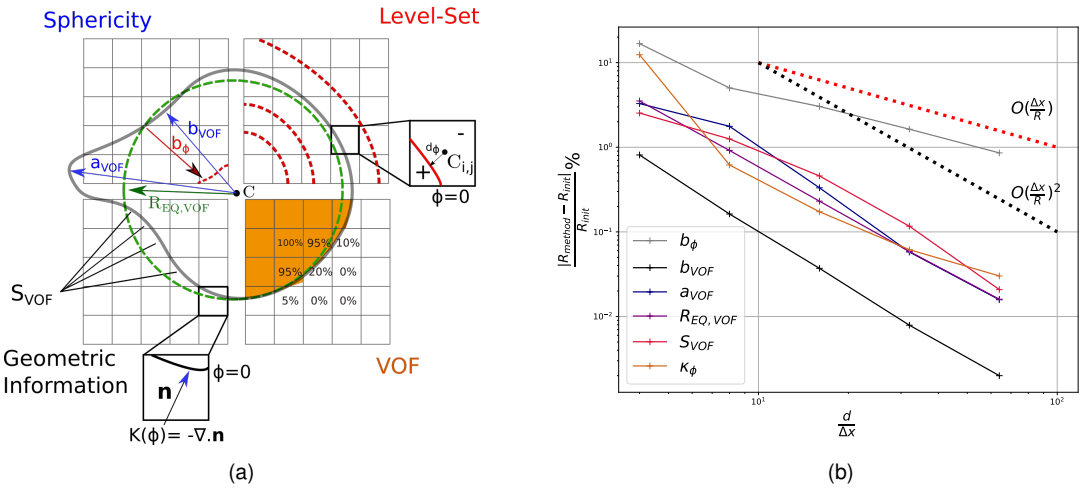

Figure 1. (a) Information from *CLSVOF* Method, top-left: sphericity, top-right: distance, down-left: geometric information, down-right: *VOF*. (b) evolution of the accuracy for each geometrical parameter increasing number of mesh in the droplet.

The information of the *CLSVOF* method can also help to determine the deformation of a structure. In particular, we can compute the maximum and minimum distance to the center, noted here a and b respectively. They are illustrated on the top left part of the figure 1a. A first method to obtain these distances is based on the volume of fluid (a_{VOF} and b_{VOF}). Based on the tag algorithm, the maximal and minimal distance from the center of the structure, $\mathbf{X}_{struct}$, to the furthest and closest cell belonging to the same structure can be obtained with a simple distance calculation. This calculation does not give the exact distance to the interface but to the cell center containing the interface. Thanks to another property of the *Level-set*, the exact distance from the cell center, $\mathbf{X}_i$, to the interface in the cell can be calculated and it is represented on figure 1a with the parameter d_ϕ. This distance calculation is shown on equation 5 for the maximal deformation, a_{VOF}.

$$a_{VOF} = \mathbf{max}_i(|\mathbf{X}_{struct} - \mathbf{X}_i| + d_{\phi,i}). \tag{5}$$

To obtain b_{VOF}, the same algorithm is used. Deformation b can also be obtained as the maximum value of the *Level-set* inside a given simple structure. It is important to notice that R_{eq}, a_{VOF} and b_{VOF} give accurate information when the center of mass is inside of the structure.

Computation accuracy of geometrical properties

In order to better understand the reliability of each distance calculation, a simple test case is run before implementation of those calculation in sphericity calculation criteria. A single 3D static droplet is initialized at rest. The diameter of the droplet is 50% the domain length. The density ratio and viscosity ratio are set to 1. The droplet is initialized in the domain with the *Level-set* function. Then, the *VOF* is computed based on the *Level-set* as described in Ménard et al. [6]. The number of cells is increased, $\frac{d}{\Delta x} = 3, 6, 12, 24, 48$, in order to determine the order of accuracy of each geometrical property. They must provide the radius of the initial droplet and errors are computed with equation 6.

$$\frac{b_{VOF} - R_{init}}{R_{init}}, \quad \frac{a_{VOF} - R_{init}}{R_{init}}, \quad \frac{a_\phi - R_{init}}{R_{init}}, \quad \frac{R_{EQ,VOF} - R_{init}}{R_{init}}, \quad \frac{R_{S_{VOF}} - R_{init}}{R_{init}} \quad and \quad \frac{R_\kappa - R_{init}}{R_{init}} \tag{6}$$

In order to analyze the influence of the initial position of a droplet with respect to the grid, 9 cases are studied by varying droplet's center on the 3D grid. The dispersion of the errors depending on the initial position has only been observed for unresolved solutions $d = 3\Delta x$. As expected, refining the mesh reduces the influence of the initial position of the droplet. Here, for comparison, we average the errors over the 9 treated cases. The evolution of the error with respect to the mesh is given in figure 1b.

From figure 1b, one can conclude that the results of the in-house code, R_{eq}, a_{vof}, b_{vof}, S_{vof} and κ_ϕ are all second order of accuracy while b_ϕ is first order. In addition to the order of accuracy, one can see that for unresolved droplet, $d \sim 3\Delta x$, b_{vof} is 40 times more accurate than b_ϕ. Thus, to study the minimal distance from the center of the droplet to the interface, b_{vof} is used in the code. A non negligible error of over 1% is observed for a_{vof}, $R_{eq,VOF}$, S_{eVOF} and κ_ϕ for unresolved droplet. This error will be considered in the deformation analysis.

Implementation of a more accurate method, [11], to determine the surface of a structure in a cell has been implemented in 2D, based on geometrical properties. This method proposed different order of accuracy but the computational cost of the second order accuracy is 10 times more expensive than current method. In addition, according to the knowledge of the author, 3D extension have not been developed yet and its implementation would be challenging. Since the computation based on the *VOF* is accurate even for unresolved droplet this extension

has not been developed. The curvature has an initial non negligible error and this is due to the averaging process which is based on the local surface area, see equation 4. It is important to recall that this global error is not related to local curvature errors, indeed, as seen on figure 1b, the method implemented is second order of accuracy. This has been shown on previous work where the Laplace-Young law was verified for a single spherical droplet at rest [12]. Geometrical parameters of the droplet are implemented in the determination of deformation criteria. These criteria are introduced in the following section.

Droplet to particle transformation criteria

The hypothesis of transformation of unresolved droplets is based on various assumption. First, droplet has to be enough isolated from other structures. Then, if the droplet is small enough, it is transformed into particle. In another hand, if the droplet has an intermediate size, $\sim 4\Delta x$, sphericity criteria are studied to ensure that the droplet is spherical enough and that it will no longer break, in order to validate particle tracking assumption.

Calculation of the deformation

In Herrmann [1], a calculation of the deformation is based on the ratio of the maximal distance from the center of the droplet to the interface, a, divided by the equivalent radius of the droplet, Req, equivalent to $\tilde{a}-1$ in this communication. In Zuzio et al. [4], they define the deformation criteria as the ratio between the minimal distance from the center of the droplet to the interface, b, divided by the equivalent radius of the droplet, Req, equivalent to $1-\tilde{b}$ in this communication. In their work, b is calculated with the *Level-set*, b_ϕ, but in our in-house code, the most accurate is b_{VOF}, then, we can not claim that our implementation is exactly the one of Zuzio et al., but it has a similar purpose. Here, we refer to the equivalent radius as $R_{EQ,VOF}$ introduced before. Both of those parameters are a global calculation and do not consider the fluctuation on the interface in their calculation. Here, two others parameters are defined based on the same geometrical parameters: the flattening and the eccentricity. See equation 7.

$$\tilde{b}=1-\frac{b}{R_{EQ}},\quad \tilde{a}=\frac{a}{R_{EQ}}-1,\quad flattening=1-\frac{b}{a},\qquad \text{and}\quad eccentricity=\sqrt{1-\frac{b^2}{a^2}} \tag{7}$$

All the deformation criteria defined in equation 7 are set in order to remain always positive and converging towards 0 when the structure is spherical. With these deformation criteria, the surface ratio and curvature ratio are implemented to obtain more information on the local surface behavior that simple deformation criteria could not provide, see equation 8.

$$\Delta\tilde{S}(\phi)=\frac{R_{S_{VOF}}-R_{EQ,VOF}}{R_{EQ,VOF}}\quad \text{and}\quad \Delta\tilde{\kappa}(\phi)=\frac{R_\kappa-R_{EQ,VOF}}{R_{EQ,VOF}}. \tag{8}$$

Here both criteria are also set in order to converge to 0 when the structure is a sphere. For some geometrical examples of the curvature criteria we refer to [13]. The mathematical definition of the sphericity of a structure of volume V and surface S is given by $\pi^{\frac{1}{3}}(6V)^{\frac{2}{3}}/S$. In the surface criteria, $\Delta\tilde{S}(\phi)$, the surface of the droplet is already compared to the volume (recall that $R_{EQ,VOF}$ is computed from the total volume of the structure). Then, $\Delta\tilde{S}(\phi)$ criteria is redundant to the sphericity. Here we study the surface criteria given in equation 8.

Lamb oscillation

Deformation of a droplet is studied on an academic test case, based on the work of Aniszewski et al. [12]. This validation case is well-known in the literature to find the linear decrease evolution of an oscillating droplet based on the Lamb's theory.

A 3D ellipsoid at rest is initialized in a 64^3 domain with 32 cells in its equivalent diameter. Physical parameters of the droplet are the surface tension, $\sigma=0.074\,N/m$, the viscosity ratio, $\mu^*=1.05$ with $\mu_{liq}=1.79.10^{-3}m^2/s$ and the density ratio, $\rho^*=10$ with $\rho_{liq}=1000kg/m^3$ The initial deformation rate of the ellipsoid is initialized with the *Level-set* function. Here, we select z as the symmetry axis, then and the initial prolate spheroid is initialized such as the major axis is 1.15 times the minor axis. Due to the capillary force, the spheroid will oscillate , going from prolate to oblate with an oscillatory period of $0.05\,s$ seconds, and, due to dissipation, tends to a spherical droplet where all deformation criteria should converge to 0.

In figure 2 the time evolution of computed criteria are given. As expected, all parameters tend to the value obtained for a sphere. The prior convergence of the error study allows us to determine the error of calculation that is made for each parameter. It is the reason why the eccentricity criteria can not reach the expected value of 0, the error made on the maximal and minimal distance is drastically amplified, an error of 1% on a and b creates an error of $\sim$10% on the eccentricity. To our purpose that is to transform unresolved droplet into particle, this criteria is too sensitive to the errors on the distance and it can not be conserved, even if the trend gives interesting information on the deformation of the ellipsoid-spheroid evolution.

The deformation criteria introduced by Zuzio et al. [4] and Herrmann [1] only characterizes variation of maximal or minimal deformation. To illustrate this point for $\tilde{a}$, we focus on the second and third oscillations on figure 2 (i.e. $t\sim 0.01\,s$ and $t\sim 0.015\,s$). According to the physical dissipation, the magnitude of the oscillation is expected to decrease. That can be observed on the flattening that decreases from 10% to 7%. Nevertheless, here we observe an increase of $\tilde{a}$. Same comment for $\tilde{b}$ at third and fourth oscillation (i.e. $t\sim 0.015\,s$ and $t\sim 0.02\,s$). Both parameters are not able to correctly estimate the decrease of the droplet's deformation and this is because they

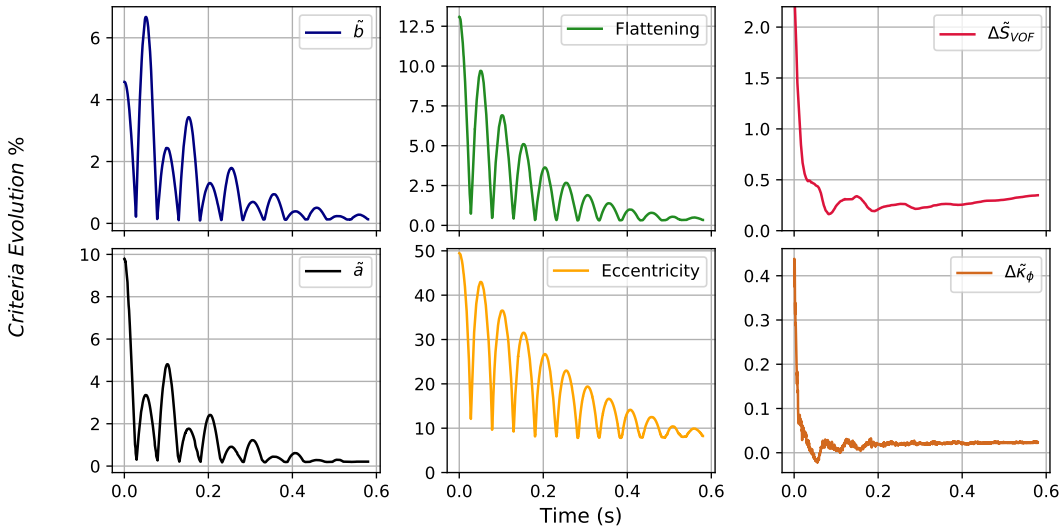

Figure 2. Evolution of deformation criteria for Lamb oscillation.

only focus on extreme values compared the equivalent radius, that is constant in this case. Then, each parameter can give different information on a structure, for example, $\tilde{a}$ can evaluate the elongation of a droplet. However, from figure 2, we can notice that for a given value of $\tilde{a}$, $\tilde{b}$, eccentricity or flattening, it is impossible to determine if the structure corresponds to an oblate or a prolate spheroid. To extract such information a combination of these parameters is necessary. Again at $t = 0.01\,s$ or other oscillations, all shape deformations are well described, as seen with the eccentricity. Our goal is to provide the criteria that describes the best the deformation, the flattening seems to be the better candidate.
Surface criteria converges to a threshold value before increasing next when the droplet is at rest. This increase remains below the error of 1% obtained in the accuracy computation, which can explain this deviation below 0.5%. It is interesting to note that from $t = 0.3\,s$, this criteria of deformation is not able to reproduce the oscillations. The evolution is more related to the local surface evolution due to local instabilities.
Curvature analysis show oscillations over and under the spherical final value. This criteria is the only one that can discriminate the prolate to oblate droplets. It can be seen that at rest, the value is still evolving. This can be due to the increase of the surface which is used to average the value of the curvature. With respect to the eccentricity which is the most sensitive method for the shape variation. The curvature shows small variations during the oscillations.
It has been seen that the magnitude of the local maxima at each period is not well described by deformation criteria introduced by Herrmann [1] and Zuzio et al. [4] which can misevaluate the shape of the droplet. In order to diminish the influence of the error and to better characterize the shape of the droplet, the flattening is conserved. This deformation criteria does not consider the equivalent radius of the spheroid reducing the sources of errors.
Nevertheless, the study of a spheroidal droplet is not enough to determine the stability of realistic droplets. In this study, we need to consider most complex droplets where the criteria based on the surface local properties, i.e. $\Delta\tilde{S}_{VOF}$ and $\Delta\tilde{\kappa}_{\phi}$, could be more relevant. The following section is devoted to the case of a droplet in a turbulent-like carrier flow.

Immersed Droplet in a HIT

The purpose of this study is to release a droplet inside of a decaying homogeneous isotropic turbulence (HIT) to observe fluctuations of velocity at the interface of the droplet and thus, local deformation. The simulation domain has 64^3 nodes, droplet diameter $\frac{\Delta x}{d} = 32$, with enough cells to reduce the error of calculation on each deformation parameter. In order to conserve one single droplet without breakage, the Weber number based on the initial velocity fluctuations is set to 1, density ratio and viscosity ratio are set to 1. Here the carrier flow is similar to the case from Tao et al. [14], with the same flow field initialization. To obtain the surrounding flow, a single phase simulation is first performed to obtain a pseudo-turbulent flow. Next, a particle is added with no slip/no penetration condition, to avoid non-physical shear at the interface when we add the droplet inside of the single phase forced flow. When the flow is established around the particle, the particle is transformed into droplet and deformation can occur in the decaying HIT. One can find more information on this process on the communication of Tao et al. [14]. Even if the turbulent flow is not fully developed, authors argue that this is not a relevant parameter for the study of geometrical parameters because we focus on the influence of the shear at the interface is our unique consideration. As it has been done before, the parameters of deformation will be compared to the equivalent radius. Their evolution must give us information on the current shape of the droplet, and its stability.
The evolution of all parameters can be split in three distinct steps, according to the results of the simulation. Those

Figure 3. From left to right, initialization ($t^* = 0$), step 1 ($t^* = 0.0005$), step 2 ($t^* = 0.0015$), and step 3 ($t^* = 0.0035$).

steps are illustrated on figure 3 with results of the droplet shape. Intermediate value for each step have been selected and initial droplet released have been added. First step, under the influence of the surrounding flow, the droplet deformation strongly increases till a local maxima at $t^* = 0.0012$. After reaching its maximal deformation, it oscillates and reaches a pseudo-equilibrum, from $t^* = 0.0012$ to $t^* = 0.003$ which is considered as the second step of the droplet's shape evolution. Step 1 and 2 on figure 3 show clearly a non spherical shape due to carrier flow influence. In third step, the droplet moves toward its spherical initial shape and the surrounding fluid will no longer deform the droplet. During this step the droplet follows simple transport within the domain with small oscillations.
On figure 4, the evolutions of all criteria with respect to the spherical shape initialization are displayed as a function of the dimensionless time $t^* = t/t_c$, where t_c is the capillary time $t_c = \frac{\mu_{carrier} V_{RMS}}{\sigma}$, and V_{RMS} the initial root-mean-square velocity of the single phase flow. All criteria are analyzed based on these three steps.

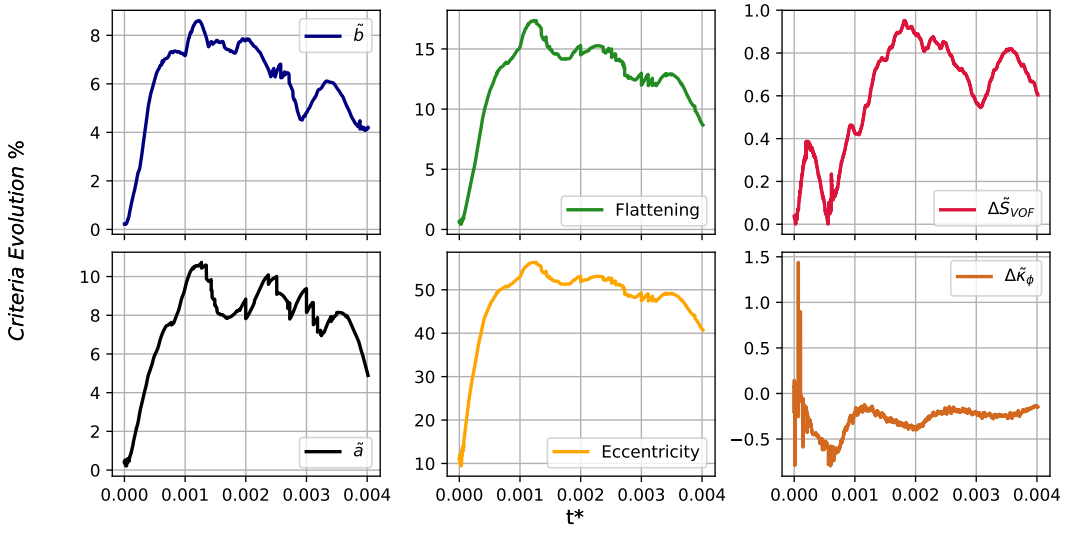

Figure 4. Evolution of deformation criteria with respect to the dimensionless time for a droplet immersed in a HIT

One can observe on figure 4 that $\tilde{a}$, $\tilde{b}$, flattening and eccentricity exhibit a similar behavior for each steps.
Those parameters increase under the motion of the surrounding flow till a maximum value at $t^* = 0.0012$, as expected, they characterize accurately the deformation of the droplet. Then, a plateau is reached and one can see small variations on the curve, representing the surface oscillations of the droplet shape, from $t^* = 0.0012$ to $t^* = 0.003$. Only noticeable difference is the order of magnitude of the variations of deformation criteria. From the simulation, we observed that the influence of the flow on the droplet only transports it during step 2 and this is mainly the reason of those variations. After $t^* = 0.003$ no breakage can then occur since the droplet is only transported.
For $\tilde{a}$ and $\tilde{b}$, maximum and minimum of variation are not synchronous, this phase difference is due to the alteration of maximum and minimum as explained for the prolate-oblate variation on the ellipsoid case. Discontinuities are observed in the time evolution of $\tilde{a}$ and not on $\tilde{b}$ which is relevant with the accuracy of each parameter seen in figure 1b. Their impact is observable on the results of the flattening and the eccentricity. Even if these discontinuities do not affect the general conclusions, improvement on this distance calculation has to be done and this could lead to have a value of eccentricity able to converge towards 0 for spherical structure.
As mentioned before, the surface and the curvature are introduced in order to highlight local surface oscillations. It can be observed that these criteria exhibit a different behavior during step 1, i.e. till $t^* = 0.0008$. This can be understood by the presence of a strong shear at the interface. During first step of ΔS_{VOF}, its evolution reaches a local maximum at $t^* = 0.0004$ and then decreases to reach minimal value. This shows that this criteria can provide other information. Our guess is that the surface criteria can provide information on the stability of the droplet determining impact of the strong shear at the interface. Nevertheless, the second step shows that similar variations are obtained compared to global deformation parameters. This criteria must be studied on a wide range of structures to determine if it is relevant. Similarly to the surface, $\Delta\tilde{\kappa}_\phi$ presents strong variations due to the initial shear

at the interface during step 1. A minimum is obtained before the second step, at $t^* = 0.0005$. Even if deformation keeps increasing, $\Delta\tilde{\kappa}_\phi$ decreases. This can be understood if we assume that the shear decreases at the interface as expected in decaying HIT. Thus, this parameter can give information on a decrease of local instabilities on the surface. It is also obersved for ΔS_{VOF} and characterizes the end of the strong increase of the deformation for other parameters. It is interesting to notice that the curvature gives negative values. This is explained because the local surface can be locally convex and is not anymore purely concave as for the previous case where the structure were assimilated to a spheroid. Shape evolutions of the droplet are well characterized by all the distance parameters and exhibit a similar behavior. For the surface and the curvature, it is complicated to extract information on the stability of the droplet. A test on a real application has to be carried out to study those criteria on a wider range of droplets and then, they could be considered as stability criteria.
In the next section the criteria are applied to an airblast atomizer and the focus will be on the surface and curvature criteria for a wide range of droplets of undetermined shapes at a selected time of the simulation. Both criteria are coupled with the flattening which is selected as a reliable criteria for the deformation.

Airblast atomizer

To apply our local and global deformation criteria on a real application, we used the results of Mukundan et al. [15] of a planar sheet airblast atomizer. Details on the configuration can be found in its communication. Here we analyze with our criteria a time step of this atomization process. The selected snapshot is given on figure 5a.

(a)

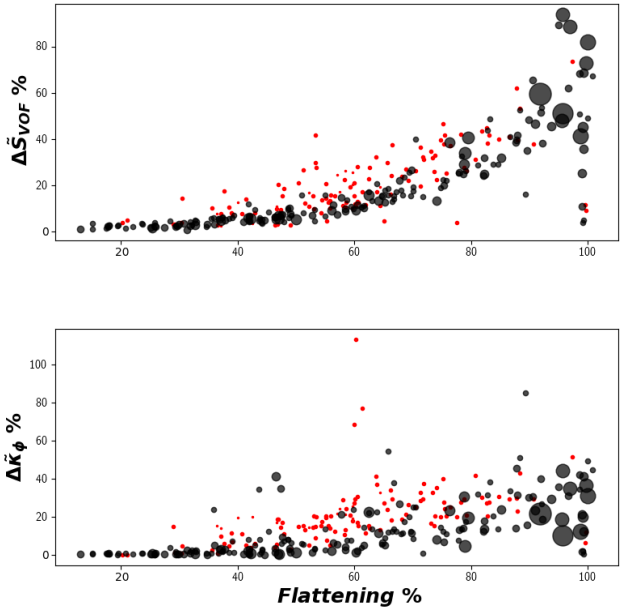

(b)

Figure 5. (a) Airblast atomizer snapshot. (b) Scatter of structures in terms of flattening, ΔS_{VOF} and $\Delta\tilde{\kappa}_\phi$

On figure 5b a scatter of the criteria selected in our previous discussion, i.e. flattening, surface and curvature, is given for all the liquid structures that are observed. The marker size represents their radius expressed in $R_{EQ,VOF}$. Red color represents the droplets below the threshold value $R_{EQ,VOF} < 2\Delta x$, according to the size criteria of Ling et al. [16] In the Eulerian-Lagrangian method these droplets are transformed due to the size criteria. In this paper, we focus on intermediate sizes.
On figure 5b top, we observe a relative clear correlation between surface and flattening going from low ΔS_{VOF} and flattening to high ΔS_{VOF} and flattening in a parabolic evolution. Large structures, defined for high $R_{EQ,VOF}$, are located next to highest flattening value. In general, these structures are large ligaments as we can observe on the snapshot of the simulation, due to their elongation, we expect such a value of flattening. It is important to recall that by definition the maximal value of the flattening is 1. These structures appear in dense regions close to the primary atomization area. According to their size, their shape and their position in the simulation, they are not considered for the transformation. We can observe that most of the small droplets that have to be transformed based on the size criteria, i.e. red marker on figure 5b, are located next to 60% of flattening. Due to their size, these droplets are not well treated by the ICM method. Nevertheless, the flattening value is too large, meaning that these droplets are not completely spherical. The Lagrangian tracking could not be as accurate as expected to transport them. Intermediate size structures are displayed all along the flattening criteria and it shows that this deformation criteria is able to select the spherical droplets in real application.
At this point of the analysis, it is complicated to conclude on the stability of a droplet from the *flattening*$-\Delta S_{VOF}$ coupling. Authors plan to go further on the analysis.
On figure 5b bottom, $\Delta\tilde{\kappa}_\phi$ scatter is provided. We can observe small droplets with unrealistic $\Delta\tilde{\kappa}_\phi$ over 60%. These

values are given by the error on computation of the geometrical proprieties. While figure on the top shows a strong correlation between ΔS_{VOF} and the flattening, the correlation between $\Delta\tilde{\kappa}_\phi$ and the flattening is less pronounced. However, below 30% of flattening, $\Delta\tilde{\kappa}_\phi$ is close to 0 and this is expected for quasi spherical droplets which are expected stable. In the future work an analysis of the droplets one by one will be done in order to better understand the role that plays the curvature in this study.

Conclusions

Geometric information on structure have been implemented in the code and their accuracy has been validated on a simple test. Then, from those geometric information, deformation criteria have been built and tested on simple case to study their evolution with respect to deformation of the shape of a spheroid and oscillations on the surface of the droplet. All of the criteria based on the distance showed a similar behavior in the representation of the deformation of the droplet. Nevertheless, the flattening has been selected because it represents most accurately the deformation of the droplet and its computation is very accurate. Different behavior have been observed for the surface and curvature criteria.

In order to go further, the three later criteria have been applied to a wide range of droplets, generated by an airblast atomizer simulation. The surface showed a similar evolution with the flattening while the curvature behavior provides less clear tendency.

Due to the definition of the surface that has been implemented in *ARCHER*, it is the most reliable criteria to determine the deformation of a droplet and to study complex geometries, nevertheless, at the current level of developments, the flattening remains the best criteria to determine if unresolved structures of intermediate size, $\sim 8\Delta x$, are spherical or not. In order to provide a better description of the deformation and the stability, the coupling between the surface and the curvature criteria is actually under study.

Acknowledgments

This work was granted access to the HPC resources of IDRIS, TGCC and CINES under the allocation A0012B1010 made by GENCI (Grand Equipement National de Calcul Intensif). The authors would thank Anirudh Asuri Mukundan for sharing its airblast numerical results and Alexandre Poux for the fruitful exchanges. We also thank the Normandy region for their funding of this research.

References

[1] Herrmann, M., 2010, Journal of Computational Physics, 229, pp. 745-759.
[2] Lefebvre, A. H., and McDonell, V. G., 2017, "Atomization and Sprays". CRC press.
[3] Shinjo, J., and Umemura, A., 2010, International Journal of Multiphase Flow, 36 (7), pp. 513-532.
[4] Zuzio, D., Estivalèzes, J.-L., DiPierro, B., 2016, Computers and Fluids, 176, pp. 285-301.
[5] Lasheras, J.C., Eastwood, C., Martínez-Bazán, C., Montañés, J.L., 2002, International Journal of Multiphase Flow, 28, pp. 247-278.
[6] Ménard, T., Tanguy, S., Berlemont, A., 2007, International Journal of Multiphase Flow, 33, pp. 510-524.
[7] Tanguy, S., and Berlemont, A., 2005, International Journal of Multiphase Flow, 31 (9), pp. 1015-1035.
[8] Vaudor, G., Ménard, T., Aniszewski, W., Doring, M., Berlemont, A., 2017, Computers and Fluids, 152, pp. 204-216.
[9] Kindlmann, G., Whitaker, R., Tasdizen, T., Möller, T., 2003, 14th IEEE Visualization, pp. 513-520.
[10] Osmar, L., Vincent, S., Caltagirone, J. P. , Estivalèzes, J. L., Auguste, F., Magnaudet, J., Ménard, T., Berlemont, A., Aniszewski, W., Ling, Y., Zaleski, S., Aug. 3-7 2014, ASME Proceedings, 2nd International Symposium on Multiscale Methods for Multiphase Flow.
[11] Müller, B., Kummer, F., Oberlack, M., 2013, International Journal for Numerical Methods in Engineering, 9 6 (8), pp. 512-528.
[12] Aniszewski, W., Ménard, T., and Marek, M., 2014, Computers and Fluids, 97, pp. 52-73.
[13] Romain, C., Puggelli, S., Essadki, M., Duret, B., Ménard, T., Massot, M., Réveillon, J., Demoulin, F.X., 2018, International Journal of Multiphase Flow, 107, pp. 230-245.
[14] Chen, T., Chéron, V., Brändle de Motta, J. C., Ménard, T., Guo, Z., Wang, L.-P., Berlemont, A., Sep. 2-4. 2019, 29th European Conference on Liquid Atomization and Spray Systems.
[15] Mukundan, A. A., Ménard, T., Berlemont, A., Brändle de Motta, J. C., Mar. 24-27 2019, 11th US National Combustion Meeting.
[16] Ling, Y., Zaleski, S., and Scardovelli, R., 2015, International Journal of Multiphase Flow, 76, pp. 122-143.